Simulation of traveling interface pulses in bistable surface reactions

Alexei Makeev[1] and Ronald Imbihl[2,*]

[1]*Faculty of Computational Mathematics and Cybernetics, Lomonosov Moscow State University, Moscow, Russian Federation*

[2]*Institut für Physikalische Chemie und Elektrochemie, Leibniz-Universität Hannover, Callinstrasse 3A 30167 Hannover, Germany*

(Received 17 July 2019; published 7 October 2019)

A couple of bistable oxidation reactions on Rh(110), the $CH_3OH + O_2$ and the $NH_3 + O_2$ reactions, exhibit localized excitations at the interface between oxygen-poor and oxygen-rich phase that propagate in a pulselike manner along the interface. A three-variable reaction-diffusion model is set up based on a mechanism that explains the localized excitations as being caused by temporary structural defects generated in the vicinity of the interface. The structural defects are a consequence of different densities of surface atoms in the oxygen-induced reconstruction phases and in the nonreconstructed (1×1) phase. One- and two-dimensional simulations show that traveling interface pulses (TIPs) exist in a region of so-called double metastability adjacent to the equistability point of the bistable system. As in the experiment, we observe triangular-shaped TIPs that move fast along the interface. Diffusional anisotropy is not required for the occurrence of TIPs. All essential features of the experiment are reproduced by the simulations.

DOI: 10.1103/PhysRevE.100.042206

I. INTRODUCTION

Chemical wave patterns on catalytic single crystal surfaces have been intensely studied in the past three decades [1–5]. They have revealed an enormous richness of phenomena including a number of phenomena that cannot be found in liquid phase reactions. The differences compared to the liquid phase can be attributed to properties that are introduced by surfaces and that are not present in the liquid phase, namely, anisotropic surface diffusion, adsorbate-induced surface phase transitions, attractive or repulsive interactions of the reactive species, and a global coupling via the gas phase in addition to the well-known diffusional coupling. One of the simplest patterns in a reaction-diffusion (RD) system is a reaction front in a bistable system [6,7]. The more stable phase pushes the less stable phase out but at the equistability point where both phases are equally stable a stationary front should result. This is common behavior also in surface reactions but recent observations made in oxidation reactions on Rh(110) revealed a unique type of behavior [8,9]. Instead of a stationary front at the equistability point, deviations from the average interface position propagated in a pulselike manner along the interface.

These traveling interface modulations (TIMs) have so far been exclusively observed in oxidation reactions with O_2 as oxidizing agent on Rh(110), in the $NH_3 + O_2$ reaction, in methanol oxidation on an unpromoted Rh(110) surface and on a surface promoted with 0.1 monolayers (ML) of vanadium oxide [8–10]. A unique property of the Rh(110) surface is its enormous structural variability; i.e., depending on the adsorbate different adsorbate-induced reconstructions are stabilized [11]. This structural variability of the Rh(110) surface has been made responsible for the unusual square-shaped chemical wave patterns found in the $NO + H_2$ reaction on Rh(110) [12,13]. After the discovery of TIMs in the $NH_3 + O_2$ reaction on Rh(110), it was suspected that the simultaneous presence of N- and O-induced reconstructions at the interface is causing the TIMs. However, the discovery of TIMs in methanol oxidation over Rh(110) ruled out this possibility.

Based on the observation with photoemission electron microscopy (PEEM) that a slowly decaying bright background remained after passage of TIMs, a modification of the Rh(110) surface either by structural or by chemical changes was concluded [9]. Since no hints for an oxidic species in this reaction system were found, the modification was attributed to structural defects which are supposed to be generated in the following way. A reconstructed surface and the nonreconstructed (1×1) surface of Rh(110) exhibit different densities of Rh surface atoms [11]. An adsorbate-induced surface phase transition between the (1×1) and a reconstructed surface will therefore be connected with a mass transport of Rh atoms and, as a consequence, with the creation of structural defects. At the interface of the bistable oxidation reactions on Rh(110), essentially a surface with a high oxygen coverage coexists with a surface with a low oxygen coverage. Any fluctuation in the adsorbate coverages at the interface will therefore be associated with a structural fluctuation and via the mass transport with the formation of structural defects. Provided that a positive feedback exists between the magnitude of the fluctuations in the surface reaction and the amount of structural defects, then an excitation mechanism is conceivable which is localized at the interface.

Shortly after the discovery of TIMs in the $NH_3 + O_2$ reaction on Rh(110), a general model has been formulated composed of the FitzHugh-Nagumo and of the Allen-Cahn models that exhibit TIMs [8]. Here we use the above sketched defect generation mechanism to formulate a realistic model for the existence of TIMs in oxidation reactions on Rh(110). This model is a skeleton model as we only consider those

*imbihl@pci.uni-hannover.de

steps that are essential for the creation of TIMs. As we will show, the model reproduces nearly all essential features of the experiment. A necessary requirement for the occurrence of TIMs was shown to be the existence of so-called double metastability (DM, also called dynamic bistability) which ensures the coexistence of oxidation and reduction fronts for the same parameters.

II. MATHEMATICAL MODEL

Our goal was to develop a simple but realistic model capable of reproducing the main experimental features of TIMs. A RD-type model is used that describes the oxidation of a molecule B on a Rh(110) surface that undergoes a reconstruction with adsorbed oxygen. The molecule B to be oxidized can be methanol, ammonia, or simply CO. We consider the following reaction steps:

$$O_2 + 2^* \leftrightarrow 2O_{ad}, \tag{1}$$

$$B + ^* \leftrightarrow B_{ad}, \tag{2}$$

$$B_{ad} + O_{ad} \rightarrow BO_{ad} \rightarrow BO + 2^* \tag{3}$$

(*denotes a vacant adsorption site).

Allowing for the diffusion of both reactants, O_{ad} and B_{ad}, one arrives at the following set of RD-type equations:

$$\frac{\partial \theta_O}{\partial t} = k_1 P_{O_2} (\theta_{*,1})^2 + \alpha k_1 P_{O_2} \theta_{def} \theta_{*,1} - k_2 \theta_O^2 - k_3 \theta_O \theta_B + D_{O,x} \frac{\partial^2 \theta_O}{\partial x^2} + D_{O,y} \frac{\partial^2 \theta_O}{\partial y^2}, \tag{4a}$$

$$\frac{\partial \theta_B}{\partial t} = k_4 P_B \theta_{*,2} - k_5 \theta_B - k_3 \theta_O \theta_B + D_{B,x} \frac{\partial^2 \theta_B}{\partial x^2} + D_{B,y} \frac{\partial^2 \theta_B}{\partial y^2}, \tag{4b}$$

$$\frac{\partial \theta_{rec}}{\partial t} = k_6 (\theta_O - \theta_{rec}), \tag{4c}$$

where

$$\theta_{*,1} = 1 - \theta_O - \theta_B, \quad \theta_{*,2} = \max(1 - 2\theta_O - \theta_B, 0), \tag{5}$$

$$\theta_{def} = \max(\theta_O - \theta_{rec}, 0), \tag{6}$$

The variables θ_O and θ_B represent the surface coverage of oxygen and of the B-type species; θ_{rec} is the degree of reconstruction. All three variables in Eq. (4) can vary in the interval from 0 to 1.

Atomic oxygen induces various reconstructions on a Rh(110) surface which are all based on the "missing row" principle [11,14]. As the O coverage increases, the surface undergoes a series of $(1 \times n)$ reconstructions ($n = 2, \ldots, 5$) in which every nth row of the close-packed [110] rows is missing. We thus have an adsorbate-induced surface phase transition, $(1 \times 1) \leftrightarrow$ reconstructed phase. In the model we only distinguish between the nonreconstructed (1×1) and the reconstructed surface with the degree of reconstruction being determined by the oxygen coverage. Furthermore, we assume that the reconstruction has no direct influence on the elementary surface processes, only indirectly through the generation of structural defects. In catalytic CO oxidation on Pt surfaces, the surface phase transitions of Pt(100) and Pt(110) were shown to be the driving force for the rate oscillations observed on both surfaces [1]. Quite generally, one can assume that a change in the surface structure is always connected with a corresponding change in the adsorption properties. For Rh(110), however, no data have been reported in the literature about different oxygen sticking coefficients, $s(O_2)$, on the (1×1) and on the reconstructed phases. Furthermore, no oscillatory behavior has so far been observed in catalytic CO oxidation on Rh(110). All this suggests that, although a difference in $s(O_2)$ will certainly exist between the (1×1) and the reconstructed phases, this difference is too small to cause any significant change in the catalytic properties of the two phases. For this reason, we focus on the influence of structural defects which are generally known to increase the reactivity of surfaces.

Since the reconstructed surface phases have a lower density of surface Rh atoms than the (1×1) surface, the phase transition requires a mass transport of Rh atoms. For formation of a reconstructed phase, Rh atoms have to be removed from the (1×1) phase which diffuse around on the surface and create structural defects. Taking into account the thermal annealing of defects, one can formulate the following differential equation:

$$\frac{\partial \theta_{def}}{\partial t} = k_7 \max(\theta_O - \theta_{rec}, 0) - k_8 \theta_{def}. \tag{7}$$

The term with the rate constant k_7 assumes that the number of created defects depends linearly on how fast the surface reconstruction $(1 \times 1) \rightarrow (1 \times n)$ proceeds. The second term describes the thermal annealing of defects as a first order process. Also, it is supposed that defects are created only when $\partial \theta_{rec}/\partial t > 0$; that is, we treat the phase transition asymmetrically with respect to the creation of defects. The physical picture behind this asymmetry is that in case of the $(1 \times 1) \rightarrow$ rec transition Rh atoms have to be expelled from the surface whereas in the transition rec $\rightarrow (1 \times 1)$, unfilled positions of substrate atoms remain if reordering is not completed. Clearly, an asymmetry exists and in the model we neglect the other type of defects, namely, the vacancies, completely. Applying the steady-state approximation to Eq. (7), a stationary value for θ_{def} is obtained as $\theta_{def} = (k_7/k_8) \times \max(\theta_O - \theta_{rec}, 0)$. However, since the second term in Eq. (4a) already has an adjustable parameter α, the ratio (k_7/k_8) can be set to 1. One arrives at Eq. (6) for the defect concentration θ_{def}. For the parameters chosen here (see below), simulations with the four-variable model showed no qualitative differences as compared to the three-variable model. For this reason, in the following, the three-variable model was exclusively used.

The concentration of defects, as defined by Eq. (6), may be nonzero only at nonstationary conditions. Under stationary conditions, $\theta_{def} = 0$ and the oxygen adsorption rate becomes the standard form, $k_1 P_{O_2} (1 - \theta_O - \theta_B)^2$. On noble metal surfaces, structural defects typically increase the oxygen sticking coefficient. It was suggested that the oxygen sticking coefficient on Rh(110) stays high despite an increasing oxygen coverage due to structural defects generated by the surface reconstructions [15]. In order to account for the promotional

TABLE I. Rate constants of the model. These are the standard values used in the simulation if not noted otherwise.

Parameter	Value at 800 K	k_i^0 (s^{-1})	E_i (kJ/mol)	Reference
k_1, O_2 adsorption	10^5	10^5 (s^{-1} $mbar^{-1}$)	0	[17,18]
k_2, O_2 desorption	4.1224×10^{-2}	10^{12}	205	[19]
k_3, Surface reaction[a]	2.9567×10^5	10^{12}	100	[20,21]
k_4, B adsorption[b]	10^5	10^5 (s^{-1} $mbar^{-1}$)	0	[15]
k_5, B desorption[b]	3.4093×10^2	10^{12}	145	[15]
k_6, Creation of defects	4	4	0	Fit
α, Influence of defects	2			Fit
$D_{O,xy}$, Oxygen diffusion[c]	25	1.71×10^9 (μm^2 s^{-1})	120	[22]

[a]For the reaction constant, the values for CO oxidation on Rh surfaces were taken.
[b]For adsorption and desorption of B, the constants were estimated from Rh(110)/CO.
[c]Oxygen diffusion coefficient in the case of isotropic diffusion. Also, we set $D_{B,xy} = 50 D_{O,xy}$.

effect of structural defects on dissociative oxygen adsorption, an additional term with the parameter α was introduced in Eq. (4a). It is assumed that the defects are isolated point defects located next to regular catalytic sites. The factor α describes the enhancement of the oxygen sticking coefficient by structural defects. In this way the term $\alpha k_1 P_{O_2} \theta_{def} \theta_{*,1}$ accounts for the additional defect-mediated pathway of dissociative oxygen adsorption on Rh(110). Under steady-state conditions, model (4) described by Eqs. (4a)–(4c) is identical to the standard model for CO oxidation on Pt-group metals [5,16].

The rate constants k_i are calculated using the Arrhenius equation: $k_i = k_i^0 \exp[-E_i/(RT_{cat})]$, where k_i^0 is the preexponential factor, E_i the activation energy, T the catalyst temperature, and R the ideal gas constant. The set of constants used in the simulations are summarized in Table I.

The simulations are all conducted for fixed values of $T = 800$ K and $P_B = 2 \times 10^{-4}$ mbar, similar to that used in the experimental study of the methanol oxidation [9]. The parameters P_{O_2}, $D_{O,xy}$, and $D_{B,xy}$ vary for different simulations.

Due to its higher binding strength on Rh(110), oxygen diffusion should be much slower than the diffusion of other species (such as CO, N, H, OH, NO, C_nH_m) which can be present on the surface during methanol or ammonia oxidation. With an activation energy of 120 kJ/mol and a prefactor of 17 cm^2/s for oxygen diffusion [22], the diffusion coefficient of oxygen can be estimated to be 25 $\mu m^2/s$ at 800 K. In order to take into account diffusional anisotropy, we use different diffusional constants in the y and x directions. For the faster diffusing B species, we set $D_{B,x} = bD_{O,x}$ and $D_{B,y} = bD_{O,y}$, with $b = 50$. It has been checked that the choice of a b value in a wide range (from 1 to 10^3) has no qualitatively significant impact on the results presented in this paper.

For calculating the propagation velocity of traveling plane waves a comoving reference frame is introduced by using a new variable, $\xi = x - v_x t$, where v_x is the unknown propagation velocity treated as an additional variable. We computed the front profiles as stationary solutions in the traveling frame by using a finite-difference discretization of a one-dimensional (1D) version of Eq. (4) subjected to a so-called pinning condition to determine the correct wave speed. The stationary solutions, both stable and unstable, were calculated with the help of a numerical continuation procedure using the pseudo-arc-length continuation algorithm based on the matrix-free Newton-Krylov method [23]. Typically, a grid with $N_x = 2000$ mesh points, a spatial step $h = 0.5\,\mu$m, and $D_{O,x} = 25\ \mu m^2/s$ were used. Tests with finer grids have also been performed, but no essential changes resulted.

Numerical solution of the two-dimensional (2D) RD equations (4) in a rectangular domain was performed by the "method of lines," wherein the partial differential equations (PDEs) were transformed to a system of ordinary differential equations (ODEs) by discretization of the spatial variables and by applying a conservative finite-difference method. A 2D square grid with space step $h = \Delta x = \Delta y$ was used for discretization. The boundary conditions are either no flux or periodic. In the following, the normalized diffusion coefficients, $d_x = D_{O,x}/h^2$ and $d_y = D_{O,y}/h^2$, are given. It was found that a space step $h \leqslant 0.5\,\mu$m was required to obtain sufficiently accurate results; therefore, the basic set of the model parameters assumes that $d_x = d_y = 100\ s^{-1}$ (assuming that $h = 0.5\,\mu$m, $D_{O,x} = D_{O,y} = 25\ \mu m^2/s$). The ODE system was integrated numerically using an implicit Jacobian-free algorithm for moderately stiff ODEs with automatic time-step size and accuracy control.

III. SIMULATION RESULTS

A bifurcation diagram of the spatially homogeneous (lumped) model is shown in Fig. 1. The diagram displays bistability with an unreactive branch, in which a high oxygen coverage inhibits adsorption of B, and a reactive branch in which both adsorbate coverages are low. Consequently, on the upper branch of the S-shaped $\theta_O(P_{O_2})$ curve at $\theta_O \geqslant 0.5$, the B-type species are absent on the surface ($\theta_B = 0$). A small but essential B coverage, θ_B, is detected only on the lower branch of the S-shaped $\theta_O(P_{O_2})$ curve. The oxygen coverage, θ_O, is very small on this branch. The spatially distributed model (4) admits a traveling front solution, a heteroclinic trajectory in the phase plane, connecting two homogeneous stable steady states of the system.

A bifurcation diagram of the 1D RD model showing the dependence of the front velocity, v_x, on the oxygen partial pressure is displayed in Fig. 2(a). This diagram has been computed using a traveling frame. Two turning points, with one of them coinciding with the equistability point, define the region of double metastability (DM). In the DM region, two different stable front solutions, the oxidation front (OF) with $v_x > 0$ and the reduction front (RF) with $v_x < 0$, coexist [24].

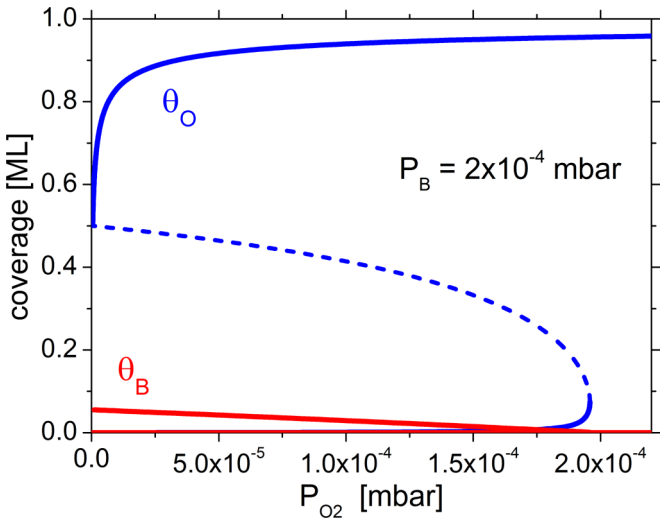

FIG. 1. Bifurcation diagram for the lumped model. Shown are the steady-state coverages θ_O (blue) and θ_B (red) as a function of the oxygen partial pressure. The stable (unstable) solutions are shown by solid (dashed) lines.

Qualitatively similar results are observed in a wide range of $b = D_{B,x}/D_{O,x}$ values (from 1 to 10^3); quantitatively, however, the difference in diffusivity has consequences because the DM region becomes shorter (wider) and shifts to the right (left) for $b > 50$ ($b < 50$). Figure 2(b) shows $v_x(P_{O_2})$ for different values of the parameters α and k_6. The parameter k_6 regulates the rates of surface reconstruction and defect formation, whereas α determines the influence of defects on the oxygen adsorption rate. Variation of k_6 and α does not change the RF velocity and also not the position of the equistability point. For $\alpha = 0$, model (4) becomes the standard model of catalytic CO oxidation on nonreconstructing noble metal surfaces without DM. Increase of α and/or decrease of k_6 produces a wider DM region, as demonstrated by Fig. 2(b).

Calculated 1D spatial profiles of adsorbate coverages and defect concentrations are presented in Figs. 3(a)–3(c). These steady-state solutions coexist for identical parameters, because the oxygen partial pressure lies within the DM region. The profiles are quite similar in shape, except the oxygen profile of the OF is slightly steeper than that of the RF. The difference between the OF and RF is caused by a different defect concentration. The defects are located near the leading edge of the front because the change in oxygen concentration causes a different degree of reconstruction which in turn generates defects. Due to the asymmetry of the surface phase transition, defects are created only in the case of the OF. The RF does not give rise to the formation of defects. The velocity of the planar RF, $v_{RF} \approx -4.6\,\mu$m/s, is about 2.7 times smaller than that of the stable OF, $v_{OF} \approx 12.35\,\mu$m/s.

Traveling interface pulses (TIPs) may form at the planar RF interface in two spatial dimensions. Here and in the following we replace the term traveling interface modulation (TIM) by traveling interface pulse (TIP) because TIP is a better description as it captures the aspect of excitability that TIPs share with conventional pulses. In the simulations they can be excited applying suitable initial conditions, e.g., by setting large enough positive values of the quantity

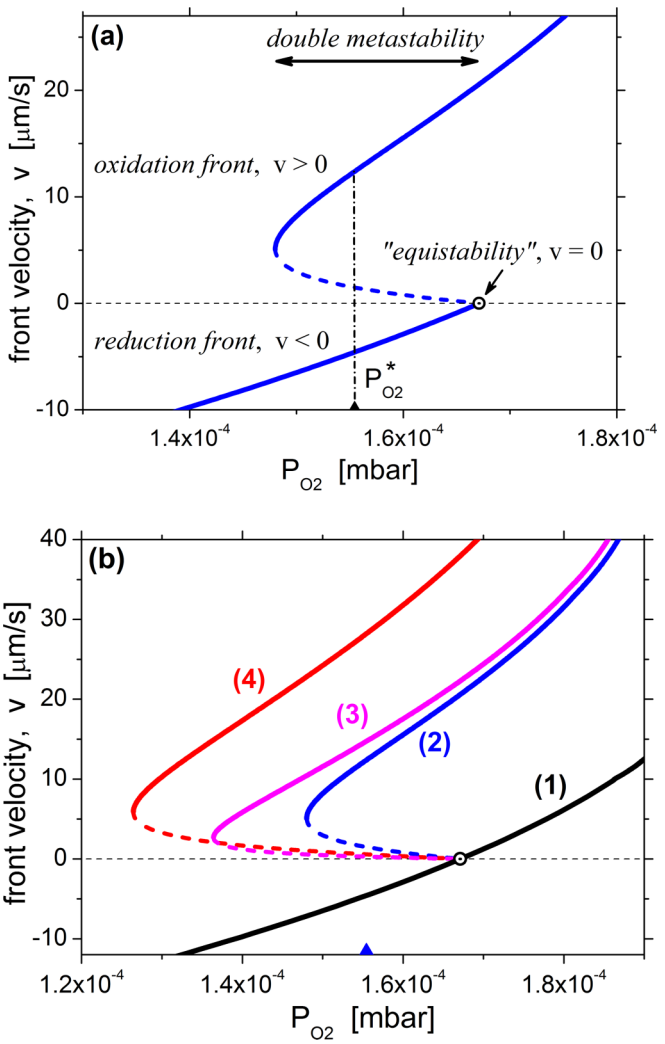

FIG. 2. Dependence of the front velocity on P_{O_2} for the 1D model with $d_x = 100\,s^{-1}$. The stable (unstable) solutions are shown by solid (dashed) lines. (a) Results for a standard set of the model parameters (Table I). In the DM region, OF and RF coexist. The dash-dotted vertical line indicates the $P^*_{O_2}$ value at which TIPs of stationary size exist in 2D simulations (see text for explanations). (b) Variation of the parameters α and k_6 (s^{-1}): (1) $\alpha = 0$, k_6, arbitrary value; (2) $\alpha = 2$, $k_6 = 4$ [coincides with (a)]; (3) $\alpha = 2$, $k_6 = 1$; (4) $\alpha = 4$, $k_6 = 4$.

$\theta_O(0) - \theta_{rec}(0)$ in a region near the interface. Figure 4 shows a typical solitary TIP which is formed due to a "bound state" of OF and RF in the DM region. In this figure and in the remainder of this paper, the following representation of 2D simulations is used. On the left (right) part of the simulated surface an oxygen-covered (nearly oxygen-free) homogeneous steady state is maintained. On the left panel the oxygen coverage distribution is color coded, using a so-called "bone" color map, from white to black. This mapping mimics the PEEM (=photoelectron emission microscopy) images where an oxygen-covered surface appears as a dark area. On the right panel of Fig. 4, the distribution of $|\theta_O - \theta_{rec}|$ instead of θ_{def} is demonstrated in order to visualize the defect-free RF interface. The defect sites, which show up as a white "stick" on the right panel, appear only near the leading edge of the OF. The OF interface length, L_{OF}, can be defined approximately

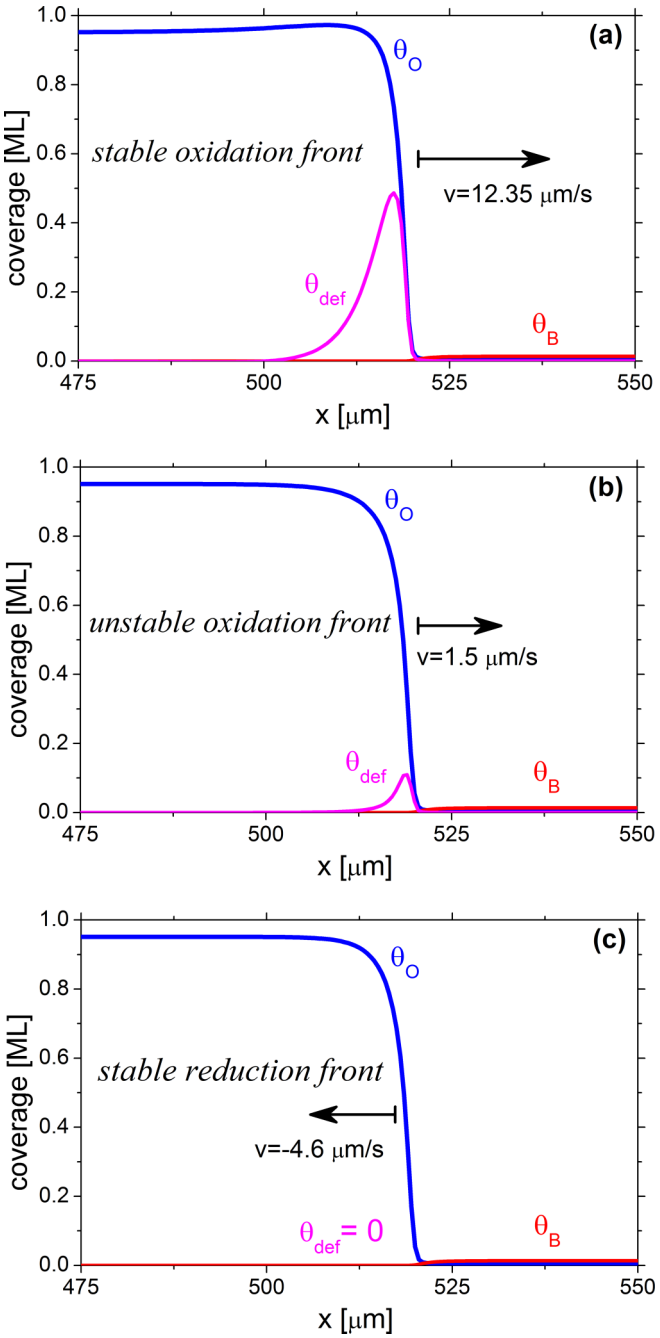

FIG. 3. Coexistence of 1D stationary front solutions: (a) a stable oxidation front; (b) an unstable oxidation front; (c) a stable reduction front. Adsorbate coverages θ_O (blue), θ_B (red) and defect concentration θ_{def} (magenta) are shown. The parameter values are $d_x = 100 s^{-1}$, $P_{O_2} = 1.554 \times 10^{-4}$ mbar.

as a length of this stick. Note that a snapshot of oxygen distribution alone does not allow one to distinguish OF and RF.

The traveling kink shown in Fig. 4 does not change its shape until it reaches the system boundaries. The interface length, L_{OF} (about 50 μm), remains constant throughout the simulation time. Similar stable structures with any $L_{OF} \geqslant 30\,\mu$m can be observed in sufficiently large systems. At higher (lower) P_{O_2} values, a growth (reduction) of the OF length takes

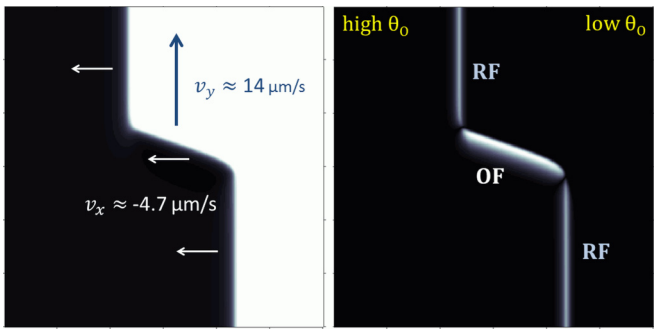

FIG. 4. Formation of TIPs on an isotropic surface. Shown is a solitary TIP consisting of two parallel "semi-infinite" planar RFs connected by an OF. A region of size $150 \times 150\,\mu m^2$ in a system of size $400 \times 1200\,\mu m^2$ with no-flux boundary conditions is displayed. The color-coded spatial distributions of θ_O (left panel; black color corresponds to a high oxygen coverage) and $|\theta_O - \theta_{rec}|$ (right panel; black color corresponds to a zero value of this quantity) are presented. The interface moves to the left with a constant velocity $v_x \approx -4.7\,\mu m/s$, and, at the same time, the kink moves up with a constant velocity $v_y \approx 14\,\mu m/s$. The parameter values are $d_x = d_y = 100\,s^{-1}$, $P_{O_2} = 1.5545 \times 10^{-4}$ mbar, $h = 0.5\,\mu m$.

place. The growth or reduction rate can be very slow and it depends on a $|P_{O_2} - P^*_{O_2}|$ value, where $P^*_{O_2} \approx 1.5755 \times 10^{-4}$ mbar is a critical value at which TIPs of stationary size exist, or, more precisely, the interface length of the TIPs is stationary. In Fig. 4 the whole interface moves to the left with a constant velocity $v_x \approx -4.7\,\mu m/s$ comprising two parallel planar RFs. Simultaneously, the kink representing an OF moves up with a constant velocity $v_y \approx 14\,\mu m/s$.

Figure 5 shows the influence of the anisotropy coefficient $A = d_x/d_y$ on the shape of TIPs. The angle β between OF and RF depends on the value of A, but β does not depend on the OF interface length, L_{OF}. Apparently, β is determined by the ratio of the planar OF and RF velocities (v_x/v_y). For a large A, β tends towards 90°, whereas a small A yields $\beta \to 180°$. In the latter case, the fast movement of TIPs along the RF resembles small "modulations" of the interface.

When periodic boundary conditions in the vertical y direction are applied, a periodic motion of the interface pulse can be observed, as demonstrated by Fig. 6. In the simulations, the structures appear stationary over a period of 10 min. During

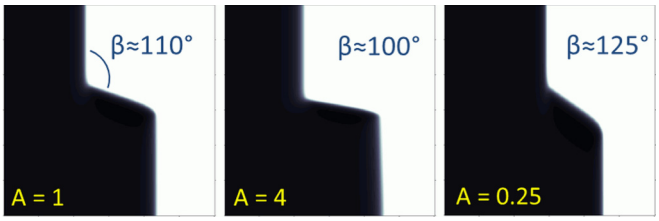

FIG. 5. Influence of diffusional anisotropy. Solitary TIPs, as given by snapshots of oxygen coverage for different values of the anisotropy coefficient $A = d_x/d_y$, at $P_{O_2} = 1.5545 \times 10^{-4}$ mbar. A region of size $150 \times 150\,\mu m^2$ is depicted. The angle β between OF and RF depends on the anisotropy coefficient A. Left panel: $d_x = d_y = 100\,s^{-1}$; central panel: $d_x = 200\,s^{-1}$, $d_y = 50\,s^{-1}$; right panel: $d_x = 50\,s^{-1}$, $d_y = 200\,s^{-1}$.

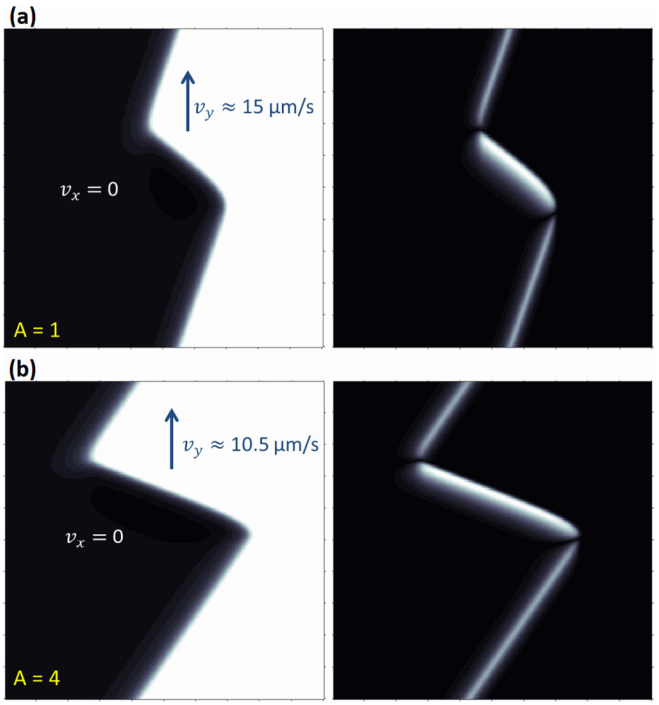

FIG. 6. Solitary TIP in an isotropic system with no-flux (periodic) boundary conditions in the horizontal (vertical) direction. The system size is $100 \times 100\,\mu\text{m}^2$; space step $h = 0.5\,\mu$m. The color-coded spatial distributions of θ_O (left panels) and $|\theta_O - \theta_{rec}|$ (right panels) are presented. (a) $d_x = d_y = 100\,\text{s}^{-1}$; $P_{O_2} = 1.5545 \times 10^{-4}$ mbar; the TIP moves up with a velocity $v_y \approx 15\,\mu$m/s, whereas $v_x = 0$. (b) $d_x = 200\,\text{s}^{-1}$, $d_y = 50\,\text{s}^{-1}$; $P_{O_2} = 1.5547 \times 10^{-4}$ mbar; the TIP moves up with a velocity $v_y \approx 10.5\,\mu$m/s, whereas $v_x = 0$. (See Supplemental Material [25], Movie 1, illustrating the evolution of TIPs.)

this time about 88 cycles in case (a) and about 63 cycles in case (b) are seen. However, such a periodic solution exists only in a narrow range of P_{O_2} values (close to $P^*_{O_2}$) and for certain initial values of L_{OF}. For larger (smaller) L_{OF} and/or for larger (smaller) P_{O_2} values, the pulse moves to the right (left) and disappears when it reaches the domain boundary. In general, the velocity of the interface along the horizontal direction depends on L_{RF}/L_{OF}, β, and v_{OF}/v_{RF}. The RF pulls the interface to the left ($v_{RF} < 0$), while the OF pulls the interface to the right ($v_{OF} > 0$). The resulting velocity of the interface in the x direction may thus become zero ($v_x = 0$) as in Fig. 6. If the vertical size of the system increases, then v_x becomes negative and a solitary TIP far from the boundaries will form as shown in Figs. 4 and 5.

Simulations on finer grids, e.g., using $h = 0.1\,\mu$m [see Fig. 7; cf. Fig. 6(b)], did not lead to essential changes in the results as compared to the case with $h = 0.5\,\mu$m. It was checked that the nearly triangular shape of the pulses seen in Figs. 4–7 is not an artifact caused by numerical approximation. Quite in contrast, the long-living trianglelike shape appears to be due to a stable connection between two different planar fronts. This connection exists even in the case of isotropic surface diffusion. During the periodic motion of the structure in Fig. 7 which was observed for $t > 3$ min, practically no change in the shape of the TIP, in its size, and in its horizontal position

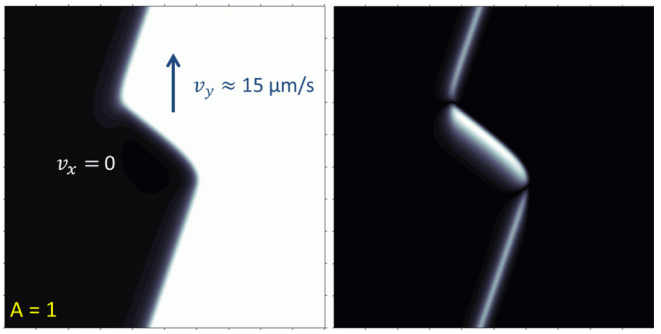

FIG. 7. Solitary TIP in a system with no-flux (periodic) boundary conditions in the horizontal (vertical) direction. The system size is $100 \times 100\,\mu\text{m}^2$; $P_{O_2} = 1.5542 \times 10^{-4}$ mbar; $h = 0.1\,\mu$m; $d_x = d_y = 2500\,\text{s}^{-1}$.

was seen (except a vertical shift). A TIP with trianglelike shape was obtained despite large values of d_x and d_y.

Besides solitary TIPs, TIP trains can be generated at the planar RF interface by choosing suitable initial conditions. In the experiment, pulse trains at the interface nucleated at macroscopic defects [9]. In Fig. 8 a TIP train combining pulses of four different shapes is displayed. This structure was excited in a system with periodic boundary conditions in the vertical direction. The simulation results for varying values of the anisotropy coefficient are displayed in three panels in Fig. 8. The average velocities of the pulses in the x and in y directions are indicated on the snapshots. Typically, v_y/v_x is in the range from 15 to 20. Very similar velocities were reported in the experimental study, e.g., $v_{[1\bar{1}0]} = 0.58 \pm 0.15\,\mu$m/s, $v_{[001]} = 16.8 \pm 2\,\mu$m/s (Fig. 3 in [9]). Due to periodic boundary conditions in the vertical direction, the pulses maintain their shape until the TIP train reaches the right boundary. The

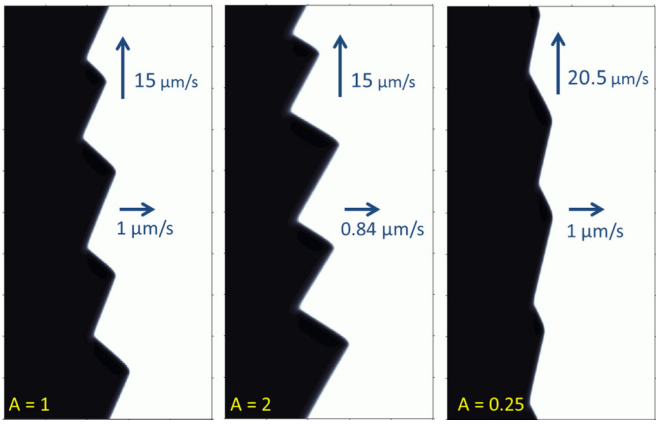

FIG. 8. TIP trains, presented by snapshots of oxygen coverage, at different values of the anisotropy coefficient A. The system size is $250 \times 500\,\mu\text{m}^2$. No-flux (periodic) boundary conditions in the horizontal (vertical) direction are applied. Each system contains four TIPs of different sizes. Left panel: $d_x = d_y = 100\,\text{s}^{-1}$, $P_{O_2} = 1.5545 \times 10^{-4}$ mbar; central panel: $d_x = 200\,\text{s}^{-1}$, $d_y = 100\,\text{s}^{-1}$, $P_{O_2} = 1.5546 \times 10^{-4}$ mbar; right panel: $d_x = 50\,\text{s}^{-1}$, $d_y = 200\,\text{s}^{-1}$, $P_{O_2} = 1.5548 \times 10^{-4}$ mbar. (See Supplemental Material [25], Movie 2, illustrating the evolution of TIP trains.)

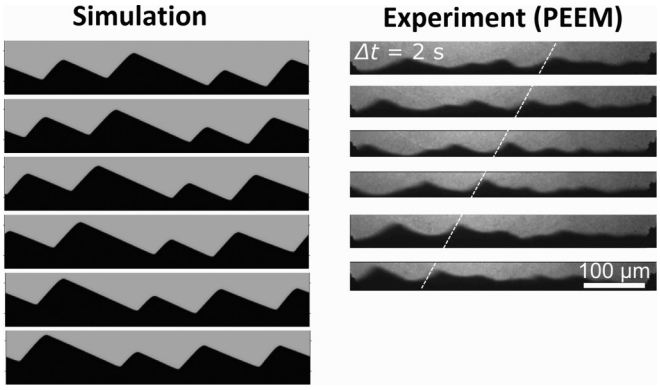

FIG. 9. Comparison of simulated (left) and experimental (right) TIPs. The experimental data taken from Ref. [9] are PEEM images recorded during methanol oxidation in the 10^{-4} mbar range on a Rh(110) surface at $T = 830$ K. In experiment and simulation, the width of the imaged area is 500 μm. The simulated TIPs (identical with simulation for left panel in Fig. 8) move to the left with a mean velocity of 15 μm/s while the whole interface shifts upwards at about 1 μm/s. In experiment, the corresponding velocities are equal to 22.1 $\pm$ 2.4 μm/s and 0.8 $\pm$ 0.1 μm/s, respectively. The diagonal dotted line marks the movement of one particular excitation. In the simulations spatial distributions of the quantity $\max(1 - \theta_O - 0.3, 0)$ are shown in a gray-scale-coded form.

net result of a TIP train is that it causes a gradual expansion of the oxidized state.

A comparison of simulated and experimental pulse trains is displayed in Fig. 9. Here the simulation data are the same as in the left panel of Fig. 8, but the snapshots of oxygen distribution are rotated by 90° counterclockwise and another color map is used. Note that the horizontal axis in the PEEM images is oriented with an angle of about 45° with respect to the crystallographic axes of the Rh(110) surface. This situation is approximately described by selecting isotropic diffusion in the simulations. In experiment and simulation, the interface pulses quickly move to the left, while the oxidized state of the surface slowly expands. The main characteristic properties of interface pulses, i.e., their shape and their velocities, are successfully reproduced by the simulations.

Simulations showed that time-periodic solutions in the form of a stable solitary TIP, like that shown in Figs. 6 and 7, exist in a very narrow range of P_{O_2} values, of about 10^{-7} mbar in width. Moreover, this narrow range may result from discretization errors, whereas the exact solution in the form of a TIP is stable only at a single value of $P^*_{O_2}$. Therefore, it would be very difficult to find such patterns in experiments. However, growing (or shrinking) TIPs can be observed in a relatively broad range of P_{O_2} values, of about 10^{-5} mbar in width. The growth rate depends on a number of factors, in particular, neighboring TIPs in a TIP train may stabilize each other, thus limiting growth or preventing destruction. In fact, PEEM experiments showed that progression of an oxidation front was accompanied by a steady growth of the TIP amplitudes [9]. Similar behavior can be reproduced by the model if P_{O_2} is chosen to be sufficiently larger than $P^*_{O_2}$. In Fig. 10 the following situation is produced. Initially, two TIPs of different amplitude were excited on the RF interface at

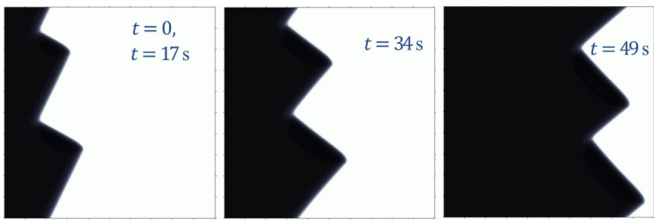

FIG. 10. Snapshots of two TIPs in a system with no-flux (periodic) boundary conditions in the horizontal (vertical) direction. At $t = 17$ s, the oxygen partial pressure is increased from $P_{O_2} = 1.5543 \times 10^{-4}$ mbar to $P_{O_2} = 1.56 \times 10^{-4}$ mbar. The system size is $250 \times 250\ \mu m^2$; $P_{O_2} = 1.56 \times 10^{-4}$ mbar; $h = 0.5\ \mu$m; $d_x = 200$, $d_y = 100\ s^{-1}$. The excitations move up with nearly constant velocity, $v_y \approx 14.7\ \mu$m/s; they also move to the right with a speed that increases with time as demonstrated by the different snapshots from left to right. (See Supplemental Material [25], Movie 3, illustrating the evolution of TIPs.)

$P_{O_2} = 1.5543 \times 10^{-4}$ mbar. The pulses maintained a periodic motion with a period of nearly 17 s in the vertical direction, while their average horizontal position underwent almost no change. Therefore, the snapshots for $t = 0$ s and $t = 17$ s are practically identical (see left snapshot). At $t = 17$ s the pressure was increased to $P_{O_2} = 1.56 \times 10^{-4}$ mbar. This P_{O_2} jump initiated a growth of TIPs and the interface started to move to the right. At $t = 34$ s (middle snapshot), the pulses have completed one cycle in the vertical direction. Meanwhile, the OF lengths of both TIPs have increased by about 25 μm. With the TIPs continuing to grow, the TIPs almost touch the right boundary at $t = 49$ s (right snapshot). This indicates that the system is close to a transition to a completely oxygen-covered state. If the horizontal extension of the system were much larger, the pulses would eventually be converted to an OF. This simulation shows that the TIPs can be observed not only when P_{O_2} is close to $P^*_{O_2}$, but also in a much wider range of oxygen partial pressures. However, a growth (reduction) of the TIP size is expected when P_{O_2} is sufficiently larger (smaller) than $P^*_{O_2}$.

It is important to note that the presence of a DM region does not guarantee that a stable TIP can be generated in a RD system. In particular, under the conditions of Fig. 2(b) [curve (2)], long-living TIPs in the DM region have not been detected. Instead, a curling of the "open ends" of the OF which destroys the nearly noncurved TIP structure has been found. A necessary but not sufficient condition for TIP formation is a large difference between the velocities of the two front types, v_{OF} and v_{RF}, e.g., a ratio v_{OF}/v_{RF} is in a range from about 2 to about 5 in Figs. 3–10. It is known that under DM conditions, the two different coexisting fronts may form a bound state (pulse) when these fronts run parallel to each other and follow one another [26,27]. Such a structure, which resembles pulses in an excitable media, can form when the two front velocities have different signs but are similar in magnitude. In this case, spiral waves or more complex (irregular) spatiotemporal patterns may appear [24,27]. The model (4) also may demonstrate such spatiotemporal patterns, but not for the parameter values investigated in this work.

In order to check the robustness of the model with respect to the choice of the constants, bifurcation diagrams like that

shown in Fig. 2(a) were constructed increasing and decreasing the standard values of the constants k_2, k_3, and k_5 in Table I by a factor of 4. In all six cases, the results are qualitatively the same: a DM region with a width of about 2×10^{-5} mbar is present and the formation of TIPs occurs in the middle of this region. Variation of the oxygen desorption rate constant (k_2) yields bifurcation diagrams that are practically indistinguishable from that shown in Fig. 2(a). A change of the reaction rate constant (k_3) has also a small effect on the results since with a large value of k_3, the surface bimolecular reaction (3) is not the rate-limiting step in the reaction mechanism. Fourfold variation of k_5 shifts the DM region by about $\pm 2 \times 10^{-5}$ mbar, but no qualitative changes are observed.

IV. DISCUSSION

Already in simple bistable systems, initially straight interfaces between two domains may undergo a number of instabilities [7]. A simple case is a linear transverse instability leading to a regular (periodic) or irregular bending of the front, but with small amplitude, which may then often be described by Kuramoto-Sivashinsky type equations [28]. If the instability does not saturate at some small amplitude, "fingering" and labyrinthine patterns may be formed [29–31]. Similar wave instabilities as in bistable systems also occur in excitable media [32]. Compared to the known instabilities at interfaces, TIPs are characterized by a fast movement along the interface, a strongly varying amplitude of the excitations, and a triangular shape. The TIPs therefore represent a unique type of stable spatiotemporal structure in a RD system. Each of the traveling interface pulses consists of an oxidation and a reduction front. The TIPs are stable in a narrow region around the point where stationary TIPs can be observed (denoted $P^*_{O_2}$ in our simulations), that is, where OF and RF are equally stable in a comoving reference frame. This point does not coincide with the equistability point of the two phases but it is located approximately in the middle of the DM range and thus not very far from the equistability point. In addition to double metastability, a stable bound state ("angle connection") of oxidation and reduction front has to exist for the occurrence of TIPs in a bistable system.

In the experiment, the usual approach was to try to reach the equistability point by varying the partial pressures but this point was never exactly met so the interface was never completely at rest but moving with a certain velocity. Experimentally, the TIPs were not restricted to a pointlike extremely narrow region in parameter space but they occurred in a parameter range of a width of less than 10% of P_{CH_3OH}. Overall, the experimental findings agree quite well with the predictions of the model. In the simulations TIPs were excited by setting suitable initial conditions. In the $NH_3 + O_2$ reaction the TIPs emanated from sharp corners of the interface but in the $CH_3OH + O_2$ reaction the sources were usually polishing scratches; that is, they are macroscopic defects.

In this paper we presented a realistic mathematical model that explains the instabilities at the interface of a bistable surface reaction as being due to the formation of temporary structural defects that enhance the reactivity of the surface. So far no direct experimental proof for the generation of structural defects at the interface exists but indirectly a number of observations strongly support the mechanism: (i) an enhanced brightness at the area passed by the TIPs that decays within a period ranging from seconds to tens of seconds and (ii) the fact that all TIPs occur in oxidation reactions with O_2 on Rh(110), i.e., in systems involving a surface phase transition whose phases exhibit different densities of surface atoms [9]. A subsequent *in situ* low energy electron microscopy (LEEM) study of methanol oxidation over Rh(110) conducted in the 10^{-5} mbar range demonstrated that in fact the oxygen-induced reconstructions (1×2), $c(2 \times 6)$, and $c(2 \times 8)$ can be found on one side of the interface while either a (1×1) or a $c(2 \times 2)$ is present on the other side of the interface [33]. The $c(2 \times 2)$ can be attributed to atomic carbon created apparently through the decomposition of adsorbed methanol. These findings confirm that a moving interface will be associated with the $(1 \times 1) \leftrightarrow$ rec phase transition.

From the above explanations, one would expect that TIP should also occur in the bistable $O_2 + H_2$ reaction on Rh(110) [34]. Under similar experimental conditions as in methanol oxidation, the $O_2 + H_2$ reaction on Rh(110) has not produced any TIPs. In the $O_2 + H_2$ reaction practically only transitions from the unreactive branch in which the surface is oxygen covered to the reactive branch with a very low oxygen coverage were observed. Transitions in the other direction were not detected—a fact that has been attributed to the equistability point lying asymmetrically in the bistability range, i.e., near one of the two saddle node bifurcations. Effectively, this means that DM is absent in this system. One simulation result of this study has been that fast diffusion of the species to be oxidized reduces the width of the DM region. This leads to the same consequence that DM is either absent or that its existence range is very small. Effectively, TIPs are not detectable in such a system.

Since the Rh(110) surface is anisotropic, the question arises whether diffusional anisotropy is essential for the formation of TIPs. In the experiment interfaces and TIPs with an arbitrary angle with respect to the crystallographic axes were found but, nevertheless, a preferential orientation parallel to the crystallographic axes existed [8,9]. The simulations showed that TIPs can also occur in systems with isotropic diffusion. The diffusional anisotropy changes the shape of the TIPs because the velocities of a reaction front being proportional $\sqrt{D_O}$ will vary differently in the x and y directions. Qualitatively, these simulation results are in agreement with the experiment.

In the experiment we found very stable high amplitude TIPs with pronounced anisotropy in methanol oxidation if the Rh(110) surface was promoted with vanadium oxide ($\approx$0.1 monolayer) [9]. The nature of the promotion effect for TIPs has not been clarified but since the principle behavior of the system did not change, one can speculate whether the VO_x enhanced the diffusional anisotropy of the surface and/or facilitated the formation of structural defects.

V. CONCLUSIONS

The main conclusion that can be drawn from the simulations is that TIPs can appear if double metastability in a bistable RD system exists. DM represents a necessary but

not a sufficient condition for the occurrence of TIPs. The characteristic features of TIPs are (1) localized excitations (pulses) may appear on the leading edge of a reduction front; (2) pulses are observed in the DM region near the equistability point of the two phases; (3) the pulses quickly propagate along a slowly moving interface; the interface separates an oxygen-covered area from a nearly oxygen-free surface; (4) the pulse size can vary to a large extent, they may grow or shrink while moving; (5) pulses may attain a nearly triangular shape. All these characteristic properties of TIPs are successfully reproduced by the simulations presented here. We therefore believe that the simulations with the skeleton model (4) strongly support the defect generation mechanism proposed as explanation for the TIPs. The model presented here should be applicable for a wide range of bistable systems where defects dynamically generated near the interface control the dynamic behavior.

ACKNOWLEDGMENT

The authors are indebted to the DFG (Deutsche Forschungsgemeinschaft) for financial support.

[1] R. Imbihl and G. Ertl, Chem. Rev. **95**, 697 (1995).
[2] H. H. Rotermund, Surf. Sci. Rep. **29**, 265 (1997).
[3] G. Ertl, Science **254**, 1750 (1991).
[4] R. Imbihl, in *Handbook of Surface Science*, edited by E. Hasselbrink and B. Lundquist (Elsevier, Amsterdam, 2008).
[5] M. Eiswirth and G. Ertl, in *Chemical Waves and Patterns*, edited by R. Kapral and K. Showalter (Kluwer, Dordrecht, 1994).
[6] A. S. Mikhailov, *Foundations of Synergetics* (Springer, Berlin, 1991), Vol. 1.
[7] L. M. Pismen, *Patterns and Interfaces in Disssipative Dynamics*, Springer Series in Synergetics (Springer, Berlin, 2006).
[8] M. Rafti, H. Uecker, F. Lovis, V. Krupennikova, and R. Imbihl, Phys. Chem. Chem. Phys. **14**, 5260 (2012).
[9] B. von Boehn and R. Imbihl, Phys. Chem. Chem. Phys. **19**, 18487 (2017).
[10] M. Rafti, B. Borkenhagen, G. Lilienkamp, F. Lovis, T. Smolinsky, and R. Imbihl, J. Chem. Phys. **143**, 184701 (2015).
[11] G. Comelli, V. R. Dhanak, M. Kiskinova, K. C. Prince, and R. Rosei, Surf. Sci. Rep. **32**, 165 (1998).
[12] F. Mertens and R. Imbihl, Nature **370**, 124 (1994).
[13] A. Makeev, M. Hinz, and R. Imbihl, J. Chem. Phys. **114**, 9083 (2001).
[14] M. Kiskinova, Chem. Rev. **96**, 1431 (1996).
[15] M. Bowker, Q. Guo, and R. Joyner, Surf. Sci. **253**, 33 (1991).
[16] M. Bär, C. Zuelicke, M. Eiswirth, and G. Ertl, J. Chem. Phys. **96**, 8595 (1992).
[17] K. A. Peterlinz and S. J. Sibener, J. Phys. Chem. **99**, 2817 (1995).
[18] E. Schwarz, J. Lenz, H. Wohlgemuth, and K. Christmann, Vacuum **41**, 167 (1990).
[19] G. Comelli, V. R. Dhanak, M. Kiskinova, N. Pangher, G. Paolucci, K. C. Prince, and R. Rosei, Surf. Sci. **260**, 7 (1992).
[20] M. J. P. Hopstaken and J. W. Niemantsverdriet, J. Chem. Phys. **113**, 5457 (2000).
[21] A. Eichler, Surf. Sci. **498**, 314 (2002).
[22] A. Makeev and R. Imbihl, J. Chem. Phys. **113**, 3854 (2000).
[23] A. G. Makeev and N. L. Semendyaeva, Comput. Math. Math. Phys. **49**, 623 (2009).
[24] M. Bär, S. Nettesheim, H. H. Rotermund, M. Eiswirth, and G. Ertl, Phys. Rev. Lett. **74**, 1246 (1995).
[25] See Supplemental Material at http://link.aps.org/supplemental/10.1103/PhysRevE.100.042206 for videos showing simulated propagation of pulses along the interface in methanol oxidation on Rh(110).
[26] A. Hagberg and E. Meron, Nonlinearity **7**, 805 (1994).
[27] M. Bär, N. Gottschalk, M. Eiswirth, and G. Ertl, J. Chem. Phys. **100**, 1202 (1994).
[28] Y. Kuramoto, *Chemical Oscillations, Waves and Turbulence* (Springer, Berlin, 1984).
[29] K. J. Lee, W. D. McCormick, Q. Ouyang, and H. L. Swinney, Science **261**, 192 (1993).
[30] R. E. Goldstein, D. J. Muraki, and D. M. Petrich, Phys. Rev. E **53**, 3933 (1996).
[31] A. Hagberg, A. Yochelis, H. Yizhaq, C. Elphick, L. Pismen, and E. Meron, Phys. D (Amsterdam, Neth.) **217**, 186 (2006).
[32] V. S. Zykov, A. S. Mikhailov, and S. C. Müller, Phys. Rev. Lett. **81**, 2811 (1998).
[33] B. von Boehn (unpublished).
[34] F. Mertens and R. Imbihl, Chem. Phys. Lett. **242**, 221 (1995).